nature electronics

ARTICLES
https://doi.org/10.1038/s41928-019-0285-3

A miniaturized multi-clamp CMOS amplifier for intracellular neural recording

Siddharth Shekar[1], Krishna Jayant[1,2,3,4]*, M Angeles Rabadan[2,4], Raju Tomer[2,4], Rafael Yuste[2,3,4] and Kenneth L. Shepard[1,3,4]*

Intracellular electrophysiology is a foundational method in neuroscience and uses electrolyte-filled glass electrodes and benchtop amplifiers to measure and control transmembrane voltages and currents. Commercial amplifiers perform such recordings with high signal-to-noise ratios but are often expensive, bulky and not easily scalable to many channels due to reliance on board-level integration of discrete components. Here, we present a monolithic complementary metal–oxide–semiconductor multi-clamp amplifier integrated circuit capable of recording both voltages and currents with performance exceeding that of commercial benchtop instrumentation. Miniaturization enables high-bandwidth current mirroring, facilitating the synthesis of large-valued active resistors with lower noise than their passive equivalents. This enables the realization of compensation modules that can account for a wide range of electrode impedances. We validate the amplifier's operation electrically, in primary neuronal cultures, and in acute slices, using both high-impedance sharp and patch electrodes. This work provides a solution for low-cost, high-performance and scalable multi-clamp amplifiers.

Intracellular electrophysiological recording from neurons is a high-fidelity neuroscience technique that enables a fundamental understanding of neuronal computation and function[1]. These recordings are typically performed using electrolyte-filled glass pipettes in either whole-cell[1] or sharp electrode[2] configurations. Pipettes used in the whole-cell configuration typically have diameters on the order of a few micrometres and impedances on the order of a few megaohms. In this configuration, the pipette tip is positioned close to the cell such that it first forms a loose seal with the membrane—commonly referred to as the 'cell-attached' configuration. On subsequent application of suction, the tip–membrane interface forms a giga-seal[1], and any further increase in the suction ruptures the membrane, yielding full intracellular access. The whole-cell technique is the current gold standard and results in precise measurement of intracellular currents and voltages. Alternatively, sharp electrodes have diameters on the scale of a few nanometres and impedances on the order of 100 MΩ and are used to impale the membrane to gain intracellular access for accurate voltage measurements. An amplifier connected to the pipette is used to control the current through the pipette and record the membrane voltage (current clamp, CC) or control the voltage in the membrane and record the membrane current (voltage clamp, VC). CC allows us to measure the voltage response of a cell to electrochemical stimuli. VC, on the other hand, can be used to determine the composition and concentration of voltage-sensitive ion channels in the membrane, which has significant implications, for example, in drug discovery.

Recording these µV-to-mV-scale voltages and pA-to-nA-scale currents necessitates the use of precision low-noise instrumentation amplifiers. The recordings are further complicated by the series resistance (R_s) and capacitance (C_p) of the pipette, which, in the best case, distort the recordings and, in the worst case, lead to a complete loss of clamping ability. The amplifier is hence also required to have associated compensation circuitry to account for these non-idealities in the pipette. Benchtop amplifiers, such as the Axopatch 200B[3] and Axopatch 700B[4], perform these recordings with high signal-to-noise ratio (SNR)[4]. However, they use discrete components in their design, increasing the cost, weight and associated wiring parasitics of these systems, which consequently limits their bandwidth, scalability, power efficiency and performance. Integrated-circuit- (IC-) based solutions can address these problems but have been difficult to realize owing to the large resistance values required in these designs, the resulting limits in the dynamic range and the limited ability to compensate for electrode non-idealities[5–10]. Nonlinear elements in feedback can be used to overcome these challenges[11]. However, these elements are extremely sensitive to variations in manufacturing and temperature, introduce distortions in the recorded data and require additional calibration circuits to account for these errors.

In this Article, we present a custom IC fabricated in a commercial complementary metal–oxide–semiconductor (CMOS) process that can perform both VC and CC measurements while overcoming many of the limitations of previous efforts. The chip includes compensation and stimulation circuitry that uses negative feedback and transistors operating in the subthreshold regime to realize large resistances. This allows us to shrink a state-of-the-art electrophysiology amplifier to an area of <9 mm^2 while consuming only 7 mW of power, several orders of magnitude lower than commercial benchtop systems. Furthermore, compared to previous efforts at multi-clamp ICs that were designed for use specifically with patch pipettes[10,11], our amplifier can also be used with high-impedance sharp microelectrodes because of its extended resistance and capacitance compensation ranges, and features a digitally programmable shared input that allows for switching between CC and VC.

Design considerations

Figure 1a presents an illustration of a typical experiment for recording intracellular signals from a neuron and a block diagram of the associated electronics. CC fundamentally consists of a voltage buffer with a high-impedance input and typically unity gain. In the special

[1]Department of Electrical Engineering, Columbia University, New York, NY, USA. [2]Department of Biological Sciences, Columbia University, New York, NY, USA. [3]Kavli Institute for Brain Science, Columbia University, New York, NY, USA. [4]NeuroTechnology Center, Columbia University, New York, NY, USA.
*e-mail: kjayant@purdue.edu; shepard@ee.columbia.edu

case where the current being injected in (I_{inj}) is zero, the only extra circuitry required is that necessary to compensate for C_p, which acts in conjunction with R_s to filter the measured signal. C_p is typically on the order of a few pF and is governed by the pipette geometry and insertion depth. However, I_{inj} is generally not zero and must be programmable in the pA–nA range. The programmability is generally achieved by varying an externally applied command voltage ($V_{command}$). When a current is being injected, R_s introduces a proportional offset voltage in the measurement. If R_s is determined accurately before the experiment and is assumed to remain unchanged, this offset is easily subtracted.

In the absence of R_s, VC is achieved using a current-to-voltage converter, also known as a transimpedance amplifier (TIA), that ensures that the pipette voltage (V_p) equals $V_{command}$ (refs. [12,13]). However, as previously noted, R_s is typically several tens of MΩ for patch pipettes[14] and can be several hundreds of MΩ for sharp microelectrodes[15,16]. Signal currents, which are typically in the pA–nA range, flow through this R_s and can cause mV-scale errors in the clamp voltage. In addition, R_s, in combination with the membrane capacitance, C_m, filters the signal of interest. Hence, dedicated circuits must compensate for R_s. C_p compensation is required to accurately determine the signal current, which is imperative for stable R_s compensation[17].

Current clamp. Figure 1b presents a detailed schematic of the CC block, which consists of a unity gain voltage buffer, C_p compensation circuitry and current injection circuitry. The voltage buffer with unity gain is implemented as an operational amplifier (op-amp) in negative feedback. The buffer must have low input leakage current so as to allow for voltage recordings with $I_{inj} = 0$. Hence, the op-amp is designed with thick-oxide metal–oxide–semiconductor field-effect transistor (MOSFET) inputs to ensure that the input leakage current is <10 fA (ref. [18]). Figure 1c shows a transistor-level schematic of the op-amp used in this design. The first stage consists of a dual n- and p-input folded cascode followed by a common-source second stage. The dual inputs enable a rail-to-rail input swing while the common-source second stage allows for a rail-to-rail output swing. The required bias voltages are generated in a separate biasing block.

C_p compensation is important for CC in order to measure voltage signals at the highest possible bandwidth. For a voltage signal V_m generated in the cell membrane, in the absence of C_p compensation, the voltage recorded by the buffer will be V_m filtered by R_s and C_p. For a patch pipette with $R_s = 25$ MΩ and $C_p = 5$ pF, this sets the 3 dB bandwidth for the recording at 1.27 kHz. For sharp microelectrodes with higher R_s and C_p, this gets proportionately worse. We achieve C_p compensation by multiplying the recorded voltage V_{buf} by a programmable factor A ($1 < A < 2$) and connecting this back to the input through a programmable capacitor C_{inj}. The current injected back in is then $(A-1)C_{inj}\frac{dV_{buf}}{dt}$. We implement A using an op-amp as a non-inverting amplifier with programmable feedback resistance that gives 10 bits of resolution (see Supplementary Section 1 for details). C_{inj} is selectable among values of 0, 5, 10 and 15 pF. The compensation step-size of $C_{inj}/1{,}024$ depends on the value of C_{inj} selected and is less than 5 fF when the 5 pF capacitor is selected.

Current injection is frequently used as a stimulus to characterize the voltage response of the cell[1]. Considering that the membrane resistance of the cell R_m is several tens of MΩ or larger, the output impedance of the current injection block needs to be at least an order of magnitude larger than this so as to not add a substantial amount of leakage current. We implement the current injection circuitry using transistors in the subthreshold regime as active current dividers, as shown in Fig. 1b[9,19]. The external $V_{command}$ is first converted into a proportional current through a fixed on-chip resistor R_{inj} (nominally 100 kΩ). This current is then passed through two stages of 32× current division to yield a net transconductance of $1{,}024 \times 100\,\text{k}\Omega \approx 100\,\text{M}\Omega$. Ratioed capacitors in parallel with the subthreshold transistors (not shown in figure) extend the operating bandwidth of the current injection. A large value for the effective injection resistance is desirable to reduce its current noise contribution, but places limits on the largest current that can be injected. The active current division utilized here serves to decrease the thermal noise of R_{inj} by a factor of N^2 such that the input-referred noise contribution of R_{inj} is then equivalent to that of a passive resistor of value ~100 GΩ (refs. [9,19]).

Voltage clamp. Figure 1d presents a detailed schematic of the VC block consisting of the TIA, the C_p compensation circuitry and the R_s compensation circuitry. The TIA achieves current amplification using similar principles to those employed in the CC current injection block for current division[20]. After two such stages provide a net current amplification of 1,024×, the current is linearly converted into a proportional output voltage using a transimpedance stage with resistive feedback. We note that while the current-to-voltage conversion in each of the current-amplifying stages is nonlinear, the op-amp ensures that corresponding sets of unit-sized transistors experience the same gate–source and drain–source voltages such that the ratio of their currents is primarily determined by the ratio of the number of devices connected between the output and the following stage to the number of devices in feedback around the op-amp, which is 32 in each of the stages in this design. Additional ratioed capacitors in parallel with the subthreshold transistors (not shown in the figure) extend the amplification bandwidth and ensure closed-loop stability for the op-amps. The feedback resistance in the output TIA stage is four-bit programmable from 0 to 225 kΩ. For large transient input currents, the output voltage of a TIA with a fixed value of feedback resistance will saturate and could lead to temporary loss of feedback. We use anti-parallel diodes in parallel with the transimpedance resistor (R) in our design to ensure that closed-loop feedback is maintained even for large input currents, at the expense of limiting the linear range of the TIA. The effective transimpedance gain of the TIA is $R_f = N^2R$. We note that it is possible to invert the diode's nonlinear I–V relationship to extend the dynamic range of our TIA, but this was not implemented in this work[11].

Another crucial advantage of our TIA is the large operating bandwidth. Traditional TIAs implemented with a large passive resistor as the feedback element are limited in bandwidth by the capacitor that is required in parallel with the resistor to ensure stability. For example, a 100 MΩ resistor in parallel with a 1 pF

Fig. 1 | Miniaturized multi-clamp amplifier. a, Typical measurement set-up for neuronal intracellular recordings. The measurement is performed in either VC or CC modes and requires different modules depending on the mode. **b**, Circuit schematic of the CC showing the implementation of the voltage buffer, C_p compensation circuitry and current injection circuitry. **c**, Transistor-level circuit schematic of the rail-to-rail input, rail-to-rail output transconductance amplifier (OTA) used in this design. **d**, Circuit schematic of the VC showing the implementation of the TIA, C_p compensation circuitry and R_s compensation circuitry. **e**, Die photograph of the amplifier IC. The chip measures 3.225 mm × 2.725 mm. **f**, Photograph of the chip assembled on a printed circuit board (PCB). The PCB measures 1.4 inch × 2 inch. **g**, Photograph of a patch pipette contacting a neuron as seen from a microscope. **h**, Photograph of the measurement set-up consisting of the microscope, manipulator and amplifier. The headstage contains all the analog components while the motherboard digitizes the analog outputs of the headstage and transmits them to a host computer (not shown).

feedback capacitor limits the TIA bandwidth to 1.6 kHz. In contrast, the feedback capacitor in the feedback path of the transimpedance stage in our design appears across R. Because this is 1,024× smaller than the effective value of the feedback resistance, the corresponding improvement in bandwidth is 1,024×. For example, this resistor would be set to 100 kΩ to realize $R_f \approx 100$ MΩ, yielding a cutoff

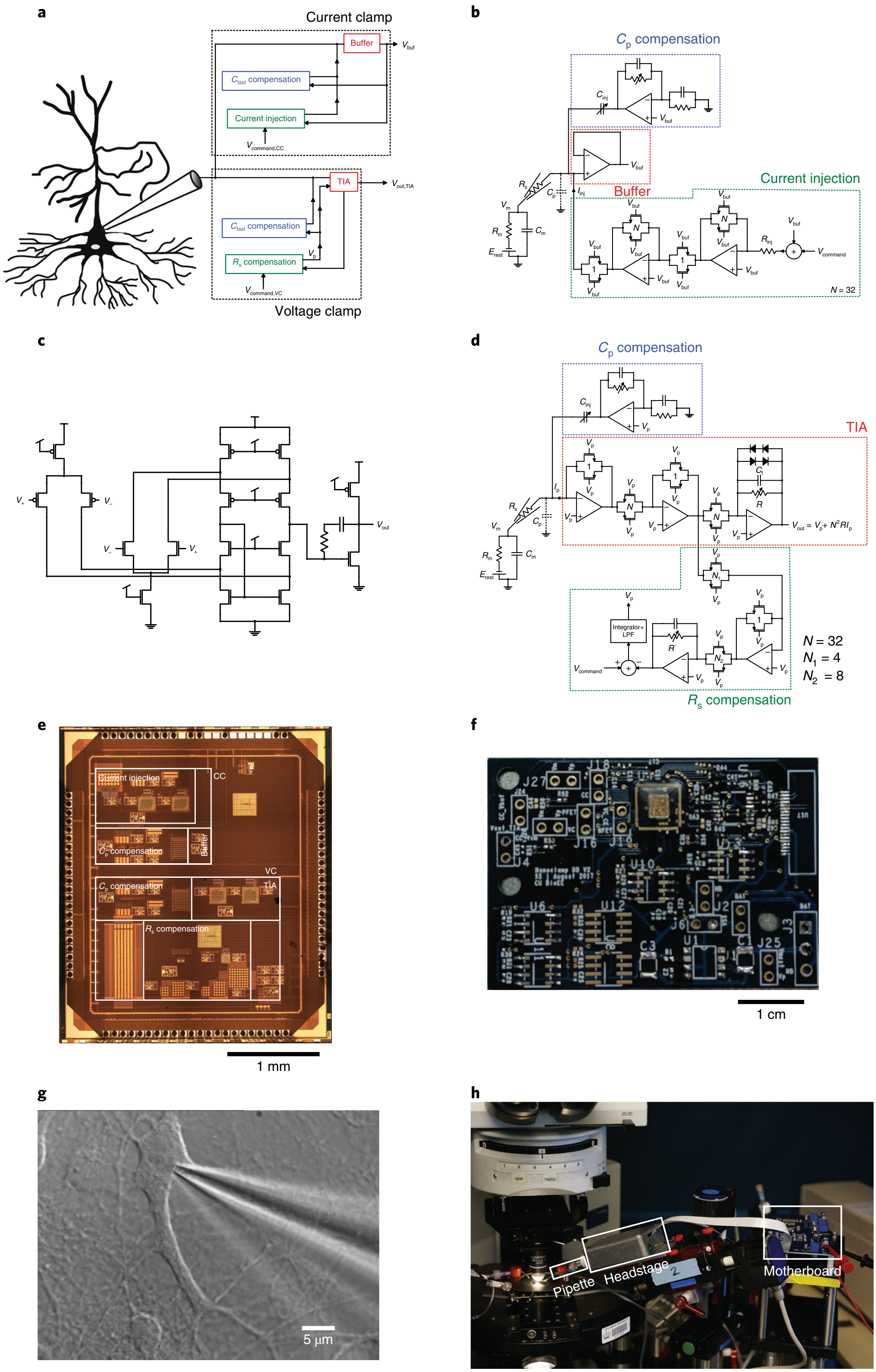

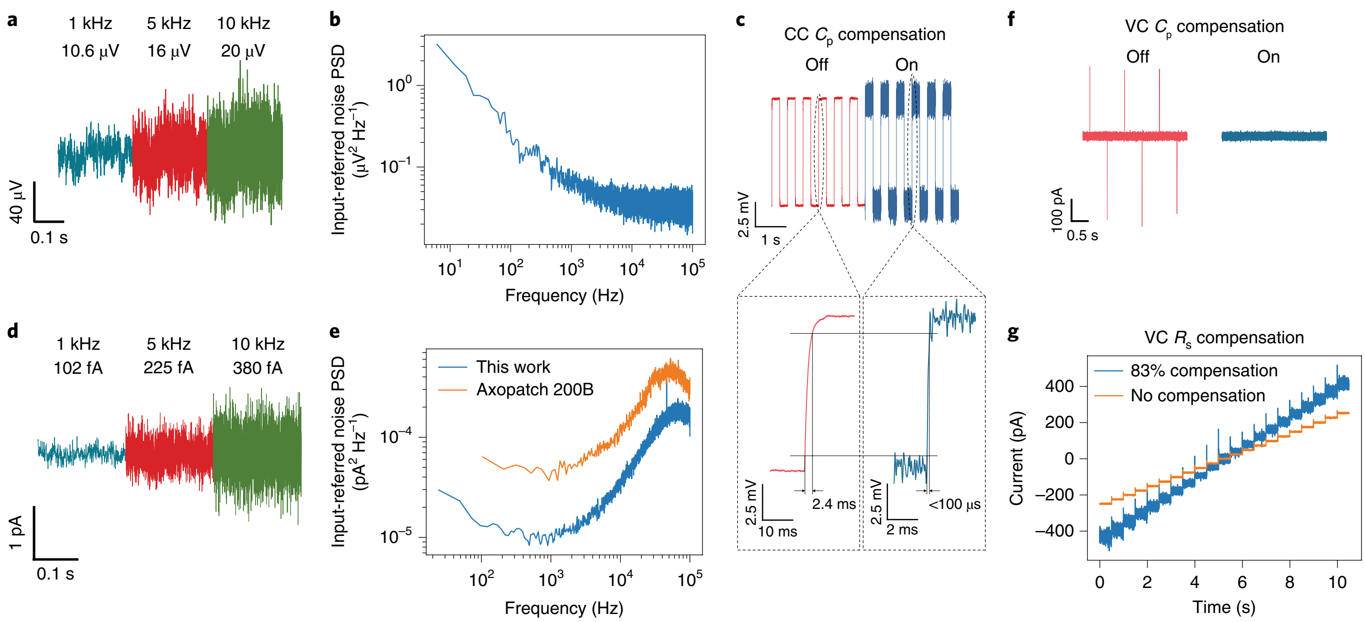

Fig. 2 | Amplifier electrical characterization. a,**b**, Concatenated 200 ms time trace (**a**) and input-referred noise PSD of an open-headstage measurement of the CC voltage buffer (**b**). The input is connected to a filtered 1.65 V source. **c**, A 10 mV$_{pp}$ square wave applied at $V_{command}$ of the CC current injection circuit generates a 10.1 mV$_{pp}$ amplitude square wave when the current is injected through $R_s = 100\,M\Omega$, indicating that the effective injection resistance is ~100 MΩ. When C_p compensation is off, the injected current is low-pass-filtered by the parasitic C_p in parallel with R_s, resulting in slow rise and fall times in the square wave. With C_p compensation turned on, the rise and fall times are reduced considerably. **d**,**e**, Concatenated 200 ms time trace (**d**) and input-referred noise PSD of an open-headstage measurement of the VC TIA (**e**). The TIA offers significantly lower noise than an Axopatch 200B ($R_f = 500\,M\Omega$). **f**, With a 10 mV$_{pp}$ square wave applied at V_p of the VC TIA, the measured current shows spikes due to the charging currents required to change the voltage across C_p. When C_p compensation is turned on, the spikes disappear completely from the recorded current. **g**, With $R_s = R_m = 100\,M\Omega$ and $C_m = 20\,pF$, without R_s compensation, the recorded current varies from −250 pA to +250 pA as $V_{command}$ is stepped from −50 mV to +50 mV in steps of 5 mV. When R_s compensation is enabled to remove ~83 MΩ of R_s, the amplitude of the recorded current increases and varies from −425 pA to +425 pA for the same waveform applied at $V_{command}$. The larger spikes at the onset of each transition in $V_{command}$ reflect the increased charging currents through C_m, which are a consequence of the reduced value of R_s.

frequency of ~1.6 MHz. In practice, however, this improvement is limited by the bandwidth of the preceding current amplification stages.

C_p compensation in VC is essential to be able to perform R_s compensation. In a typical VC experiment, V_p is stepped from its initial value at the resting membrane potential to a different value. Given that the TIA will ensure that this step is also applied at the electrode connected to the pipette, the resultant current measured by the TIA will be a combination of the desired current through the pipette and the charging current required for changing the potential across C_p. We use a replica of the C_p compensation block used as part of CC to cancel out the latter contribution.

Lack of R_s compensation would lead to three primary deviations from the desired VC behaviour[3]. First, a step change in $V_{command}$ results in a change in the membrane potential (V_m) with an exponential time constant determined by R_sC_m. Second, a current I_p flowing through R_s will cause V_m to deviate from $V_{command}$ by I_pR_s. Finally, any signal current will be low-pass-filtered with a time constant given by R_sC_m. In a typical VC experiment in whole-cell configuration with $R_s = 25\,M\Omega$ and $C_m = 30\,pF$, this would set the 3 dB cutoff of this filter at 212 Hz. A 90% compensation of this R_s can increase the measurement bandwidth by a factor of 10 to 2.12 kHz.

To mitigate these deleterious effects, our design includes R_s compensation circuitry based on state estimator theory[21]. In short, we estimate V_m as $V_{m,est} = V_p - I_pR_{s,est}$, where I_p is the current flowing through R_s once C_p has been compensated, and $R_{s,est}$ is the local estimate of R_s. We exploit CMOS matching techniques to feed an accurate copy of the current sensed by the TIA to the R_s compensation circuitry, which, in essence, is a TIA itself with 10 bit programmable feedback resistance from 0 to 256 kΩ. Combined with the 1,024× amplification in the current domain, this allows us to tune the value of $R_{s,est}$ up to 262 MΩ. The $V_{m,est}$ thus generated is then forced to equal an off-chip $V_{command}$ using negative feedback provided by an integrator implemented using a 5 bit programmable transconductance block and a fixed 64 pF capacitor. Additional programmable low-pass filters are included to help stabilize the overall loop. Achieving >75% R_s compensation is challenging[21], as I_p must be measured accurately at high bandwidths (typically exceeding 100 kHz). The circuitry used for measuring I_p and generating $V_{m,est}$ is similar to that used in the TIA and enjoys the same bandwidth benefits. Furthermore, depending on the cell membrane capacitance, our implementation allows for potentially compensating 100% of R_s (see Supplementary Sections 2 and 3 for details).

Electrical characterization

Figure 1e shows a die photograph of the 3.225 mm × 2.725 mm amplifier chip as manufactured in a 0.18 µm bulk CMOS process. The die is directly mounted on, and wirebonded to, a 1.4 inch × 2 inch custom-designed PCB. The die is then encapsulated with epoxy (see Methods) to mechanically protect the wirebonds (Fig. 1f). A connector is included to connect to conventional pipette holders for use in patch experiments (Fig. 1g). Finally, the aluminium enclosure for the PCB is designed to maintain compatibility with systems designed for commercial multi-clamp systems (Fig. 1h).

We first validated CC and VC functionality by using an electrical model cell as shown in Fig. 1b,d, with $R_s = 100\,M\Omega$, $R_m = 100\,M\Omega$ and $C_m = 20\,pF$ for VC testing, and $R_m = 0$ for CC testing, unless noted

Table 1 | Comparison to the state of the art

	MultiClamp 700B (ref. [4])[a]	Ref. [10]	Ref. [11]	This work
Type	Discrete	IC	IC	IC
Technology	–	0.5 µm silicon-on-sapphire	0.35 µm CMOS	0.18 µm CMOS
Die size	–	4 mm × 8 mm	4.7 mm × 3.0 mm	3.23 mm × 2.73 mm
Supply voltage	–	3.3 V	–	3.3 V
Power consumption	30 W[b]	30 mW[c]	–	7 mW
C_p compensation range	0–36 pF (VC) −8–16 pF (CC)	0–10 pF	0–10 pF	0–15 pF
Input-referred voltage noise in CC	–	150 μV_{RMS} in 5 kHz	8.2 μV_{RMS} in 10 kHz	20 μV_{RMS} in 10 kHz
VC TIA gain	50 MΩ–50 GΩ	49 kΩ–100 MΩ	Nonlinear[d]	0–225 MΩ
Input-referred current noise in VC (in 5 kHz)	0.8 pA_{RMS}	3.3 pA_{RMS}	1.1 pA_{RMS}	0.23 pA_{RMS}
R_s compensation scheme	Positive feedback	Positive feedback	Positive feedback	Negative feedback
R_s compensation range	0.4–744.7 MΩ	0–100 MΩ	0–32 MΩ	0–262 MΩ

[a]Values reported for $R_f = 500$ MΩ. [b]The MultiClamp 700B contains several peripheral circuits for enabling industry-standard functionality. The power reported here includes that consumed by these circuits as well. [c]Per channel power consumption. The chip contains four independent channels. [d]A diode is used as the transimpedance element.

otherwise. C_p is largely determined by the parasitic trace capacitance to ground on the PCB. We first determined the noise performance of the CC voltage buffer alone. Figure 2a shows an example output time trace for a d.c. voltage source connected to the input, filtered to different bandwidths after acquisition, and Fig. 2b shows the corresponding input-referred voltage noise power spectral density (PSD) of the unfiltered time trace. In a 10 kHz bandwidth, the root-mean-squared (RMS) value of the input-referred voltage noise is 20 μV_{RMS} and is dominated by the noise from on-PCB components. This yields an acceptable SNR for recording extracellular action potentials and offers comparable performance to commercial instruments and previous integrated efforts (Table 1).

Figure 2c shows the voltage recorded by the buffer (with and without capacitance compensation) for a 10 mV_{pp} amplitude square wave at 2 Hz applied to $V_{command}$ to inject a current square wave with a nominal amplitude of 100 pA_{pp} into R_s. The recorded amplitude of 10.1 mV_{pp} for the square wave indicates that the injected current is 10.1 mV_{pp}/100 MΩ = 101 pA_{pp}. Without capacitance compensation, the injected current is filtered by the parallel combination of R_s and C_p and, consequently, the measured voltage signal exhibits 10–90% rise and fall times of ~2.4 ms. We then tuned the C_p compensation to speed up the rising and falling edges of the transitions. With both current injection and capacitance compensation on simultaneously, we observe rise and fall times of less than 100 µs, significantly faster than the case without C_p compensation. C_p compensation operates identically for a voltage applied at V_m instead of $V_{command}$ (see Supplementary Section 4 for details).

After characterizing the frequency response and linearity of the TIA (see Supplementary Sections 5 and 6 for details), we determined the noise performance of the TIA. In VC mode, the current measured by the TIA is given by $I_p = (V_{out,TIA} - V_p)/R_f$ (Fig. 1d). With R_f set to ~225 MΩ, Fig. 2d plots the time trace of I_p for a constant externally applied V_p filtered to different bandwidths in software and Fig. 2e plots the corresponding PSD. Figure 2e also shows the input-referred noise PSD for an Axopatch 200B (Molecular Devices) with R_f set to 500 MΩ, the current commercial state of the art for low-noise ion channel recordings. Our TIA generates only 225 fA_{RMS} of noise when filtered using a fourth-order 5 kHz Bessel filter. This is a factor of three better than the Axopatch 200B. Furthermore, this is the lowest reported noise among all integrated multi-clamp efforts (Table 1 and Supplementary Section 7).

Figure 2f shows the current recorded by the TIA (filtered to 10 kHz bandwidth) with and without C_p compensation for 1 Hz,

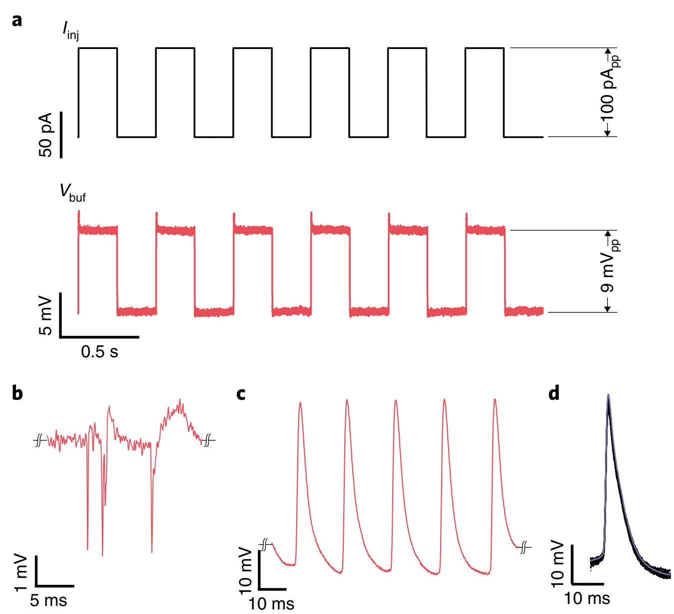

Fig. 3 | In vitro recordings using sharp microelectrodes. a, Injecting a 100 pA_{pp} current through a sharp microelectrode with slight C_p overcompensation yields a measured voltage square wave with an amplitude of 9 mV_{pp} indicating that the pipette resistance is ~90 MΩ. **b**,**c**, Extracellular (**b**) and intracellular (**c**) action potentials recorded from a neuron using the sharp microelectrode characterized in **a**. **d**, The spike-triggered average of 11 action potentials recorded using a MultiClamp 700B reveals that the recordings in **c** show similar SNR, amplitudes and timescales as those performed using the 700B.

10 mV_{pp} steps in $V_{command}$. Before enabling C_p compensation, the current waveform has large transient spikes at the onset of each step change in $V_{command}$ due to the charging currents associated with changing the potential suddenly across the parasitic C_p. When tuned correctly, the transient charging currents can be removed completely from the recorded current. In our set-up, we tuned the compensation circuitry to remove ~2 pF of parasitic capacitance.

After completely eliminating the effect of C_p, we tested the functionality of the R_s compensation circuitry with R_f set to 60 MΩ and

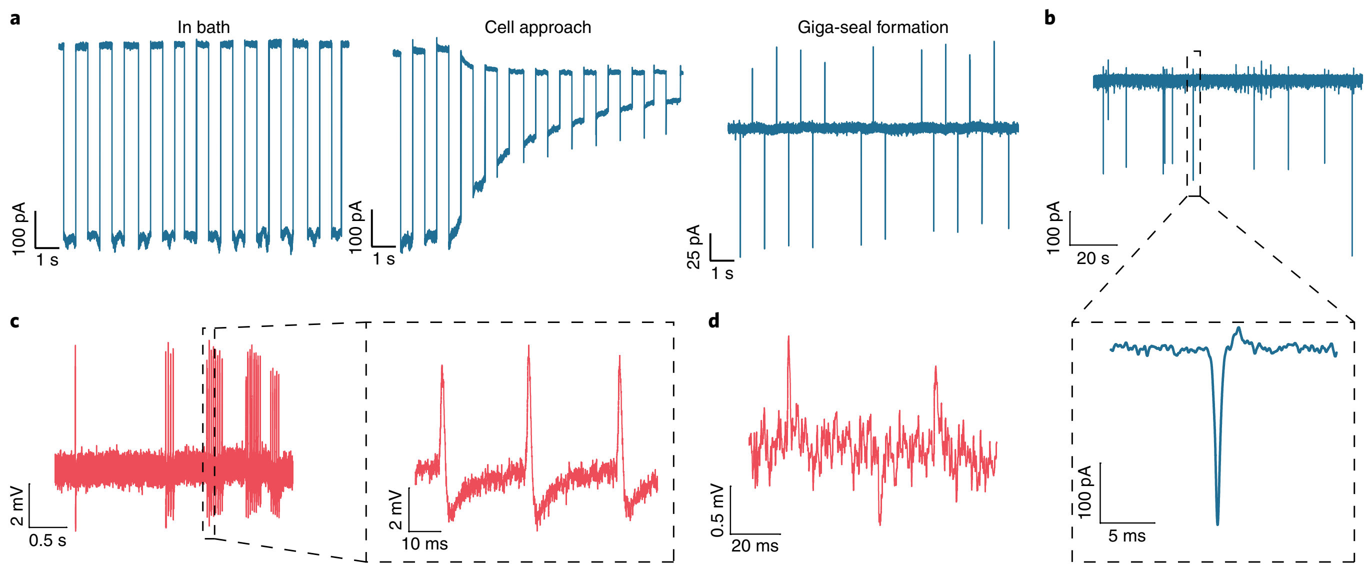

Fig. 4 | In vitro recordings using patch pipettes. a, With a 5 mV square wave applied at $V_{command}$, the current recorded by the TIA is maximum when the pipette is in the bath and decreases as the pipette approaches the cell and suction is applied. When the giga-seal is formed, there is negligible d.c. current flowing through the pipette. **b**, Loose-seal VC recording from a neuron, showing several spontaneous action potentials over the course of several seconds of recording. The magnified trace reveals high SNR and millisecond timescales. **c**, Tight-seal recordings of action potentials. **d**, Excitatory and inhibitory postsynaptic potentials from a neuron in CC.

the compensation tuned to reduce R_s by 83 MΩ. We ramped $V_{command}$ from −50 mV to +50 mV in steps of 5 mV and measured the current recorded by the TIA (Fig. 2g). In the absence of R_s compensation, the TIA applies this waveform across $R_s + R_m$, resulting in the current varying from −250 pA to 250 pA in steps of 25 pA. Enabling R_s compensation increases the amplitude of the current step to 42.5 pA, yielding an effective R_s of ~17 MΩ, indicating that the R_s compensation circuit was successful in cancelling over 80% of the original R_s as expected. The spikes at the onset of each transition shown in Fig. 2g are more pronounced when R_s compensation is enabled. As the effective value of R_s decreases because of active compensation, the voltage applied across C_m more closely resembles the desired ideal step and results in larger charging currents. If the value of C_m is on the order of tens of fF, it is possible to completely compensate for R_s (see Supplementary Section 3 for details).

In vitro characterization in cultures and slices

To validate the amplifier's functionality for neuronal measurements in both cultures and slices, we enclosed the PCB containing the IC in an aluminium box that acted as a Faraday cage. We then mounted this box on a manipulator housed within a custom-designed microscope set-up (Fig. 1h). We first characterized R_s and C_p of sharp microelectrodes for use in the CC mode by injecting a 2 Hz, 100 pA_{pp} signal into the electrode. Figure 3a shows a typical voltage response obtained with a 100 nm high-impedance sharp microelectrode (3 M KCl filling solution[22]) immersed in a bath containing artificial cerebrospinal fluid (ACSF) with the C_p compensation circuitry tuned to cancel 8 pF of parasitic capacitance. The response (filtered to 4 kHz) indicates a measured resistance of 90 MΩ with slight C_p overcompensation. We then used this electrode to perform intra- as well as extracellular recordings from cortical layer-5 pyramidal neurons in acute slices (see Methods for details). We observed a resting membrane potential of −58 mV and distinct extracellular (prior to cell entry) and intracellular neuronal action potentials with high SNR, millisecond timescales and ~50 mV amplitudes, as shown in Fig. 3b,c. We also performed recordings using the MultiClamp 700B (Molecular Devices), which is a widely used high-performance commercial multi-clamp amplifier. Our recordings compare favourably to those made using the MultiClamp 700B (spike-triggered average of 11 action potentials, Fig. 3d) in terms of SNR, timescales and signal fidelity.

In VC mode, a periodic pulse with an amplitude of 5 mV and frequency of 1 Hz was applied to determine the pipette's resistance before cell entry. The pipettes we tested in this work had resistances ranging from 7 to 14 MΩ. Figure 4a shows the current recording (filtered to 1 kHz bandwidth) through one such pipette in the bath, as it approaches the cell in three-dimensional (3D) cultures (see Methods for details) and after formation of the giga-seal. In the cell-attached configuration (loose-seal; seal resistance of ~150–200 MΩ), we held the pipette at −70 mV and observed several spontaneous action potentials, as shown in Fig. 4b (filtered to 2 kHz bandwidth). In a separate experiment we were able to observe spontaneous action potentials in CC as well (Fig. 4c, filtered to 10 kHz bandwidth). Current was injected to maintain ~−50 mV in the pipette. The signals are characterized by high-SNR biphasic waveforms and amplitudes of several mV, indicating that these were tightly coupled extracellular action potentials due to incomplete rupture[23,24]. On rupturing the membrane further, and when filtered to 2 kHz bandwidth, we were also able to observe excitatory and inhibitory postsynaptic potentials (Fig. 4d).

Conclusion

We have presented a miniaturized multi-functional CMOS amplifier chip with complete VC and CC capabilities. In doing so, we have leveraged the advantages afforded by modern commercial CMOS processes to shrink a benchtop system down to an area of <9 mm^2. In vitro, the amplifier was able to record signals with high fidelity in both VC and CC modes. The comparison with previous work shown in Table 1 shows that our system consumes the least amount of power while offering performance equalling or exceeding that of benchtop systems.

Although we have reported a single-channel system here, this approach allows scale-up of the design to support either multiple channels on the same chip or multiple chips on the same PCB.

This could open up experiments previously rendered infeasible by the physical form factor of the headstages of commercial recording systems. Furthermore, the use of a standard fabrication process allows the cost of these systems to be driven down substantially.

Methods

Amplifier chip fabrication and packaging. The amplifier chip was designed in a commercial 0.18 µm CMOS process. The chip was directly wirebonded to the PCB. This approach eliminates the standard package–socket interface and helped reduce parasitics at the input nodes. The chip was attached to the PCB using Epo-Tek H20E (Epoxy Technology) and the landing pads on the PCB were cleaned by immersion in BPS-106 (Versum Materials) for 10 min before wirebonding. After the wirebonding was complete, the chip was encapsulated using Epo-Tek OG116-31 (Epoxy Technology) to protect the wirebonds from damage during handling.

The PCB consisted of the bias current sources required by the chip, digital-to-analog converters to generate the various control voltages and analog voltage buffers. This PCB was connected via flexible ribbon cables to another PCB housing anti-aliasing filters (four-pole, 100 kHz, Bessel), an analog-to-digital converter (six-channel, 16 bit) and digital isolators. A field programmable gate array was then used to transfer the digitized data to a host PC over a standard USB 2.0 interface. We also developed a custom graphical user interface for controlling the amplifier chip and visualizing the data. All software running on the host PC was written in Python using the PyQt design framework, which allowed for cross-platform operation.

2D and 3D cell culture preparation. Animal handling and experimentation were carried out according to the US National Institutes of Health and approved by the Institutional Animal Care and Use Committees of Columbia University. Following standard procedures with minor modifications[25,26], hippocampal neuronal cultures were generated from E19 mice. Briefly, pregnant mouse were anaesthetized and euthanized by cervical dislocation. Hippocampus was dissected in Hibernate E (Gibco) ice cold medium and subsequently incubated in 0.25% Trypsin-EDTA (Gibco) at 37 °C for 30 min + 1 µg ml^{-1} DNAse I (Sigma) at room temperature for 5 min. The hippocampus was mechanically dissociated by pipetting with a fire-polished glass Pasteur pipette until a homogeneous cell suspension was obtained. Cell viability was determined by a Trypan Blue exclusion assay. The cell solution was then centrifuged at 150*g* for 10 min and the supernatant removed. The cell pellet was resuspended in culture medium consisting of neurobasal medium +2% B27 +0.5 mM glutamate +1% penicillin/streptomycin (Gibco). Between 8×10^4 and 1×10^5 cells were plated onto 12 mm poly-L-lysine-coated coverslips for 2D neuronal cell cultures. For neurospheres cultures[26], 1.5×10^6 cells were seed in poly-dimethylsiloxane (PDMS) customized moulds with a well of dimensions 50 mm × 28 mm. PDMS moulds were fabricated in 3D printed acrylonitrile butadiene styrene (ABS) cast and polymerized overnight at 90 °C. Both 2D neuronal and neurospheres cultures were incubated in culture medium at 37 °C and 5% CO_2. Experiments were performed between 14 and 21 days in vitro.

Slice preparation. Slices were prepared using previously established protocols[15]. For acute slice experiments, coronal sections of the neocortex of P7 to P20 old C57BL/6 mice of both sexes were prepared using a Leica VT1200S vibratome. The animal was decapitated (following deep anaesthesia via inhalation of isoflurane in animals older than P12), and the brain quickly removed. Slices of 300 µm thickness were prepared in ice-cold slicing solution containing (in mM): 93 *N*-methyl-D-glucamine, 2.5 KCl, 1.2 NaH_2PO_4, 30 $NaHCO_3$, 20 HEPES, 25 glucose, 5 Na-ascorbate, 3 Na-pyruvate, 10 $MgSO_4$, 0.5 $CaCl_2$; pH adjusted with HCl to 7.3, bubbled with 95% O_2 and 5% CO_2. After a short recovery period (4–8 min) in 35–37 °C warm slicing solution, slices were kept at room temperature in ACSF until transferral into a recording chamber.

Slice electrophysiology. Neuronal slices were visualized using an Olympus BX50WI microscope equipped with oblique illumination and a water immersion ×40/0.8 NA objective (Olympus). Whole-cell recordings (pipette resistance ~7 MΩ) were obtained using pipettes pulled from borosilicate glass (1.5 mm and 1 mm outer diameter, 0.86 mm and 0.5 mm inner diameter, Sutter Instruments) and established using our custom-designed amplifier. The external bath of ACSF contained the following (in mM): 126 NaCl, 26 $NaHCO_3$, 1.145 NaH_2PO_4, 10 glucose, 3 KCl, 2 $MgSO_4$ and 2 $CaCl_2$; osmolarity of ~300 mOsm. Patch pipettes were filled with internal solution containing (in mM): 130 K-gluconate, 5 NaCl, 2 $MgSO_4$, 10 HEPES, 5 EGTA, 4 MgATP, 0.4 Na_2GTP, 7 Na_2-phospocreatine, 2 pyruvic acid, 0.002–0.01 Alexa 488; pH adjusted to 7.2, ~280–290 mOsm.

Data availability

The data that supports the plots within this paper and other findings of this study are available from the corresponding author upon reasonable request.

Received: 18 December 2018; Accepted: 17 July 2019;
Published online: 15 August 2019

References

1. Sakmann, B. & Neher, E. *Single Channel Recording* 2nd edn (Springer Science & Business Media, 1995).
2. Purves, R. D. *Microelectrode Methods for Intracellular Recording and Ionophoresis* (Academic Press, 1981).
3. *Axopatch 200B Patch Clamp—Theory and Operation* (Axon Instruments, 1999); https://www.autom8.com/wp-content/uploads/2016/07/Axopatch-200B.pdf
4. *MultiClamp 700B Amplifier* (Molecular Devices, 2017); https://www.moleculardevices.com/systems/conventional-patch-clamp/multiclamp-700b-microelectrode-amplifier
5. Laiwalla, F., Klemic, K. G., Sigworth, F. J. & Culurciello, E. An integrated patch-clamp amplifier in silicon-on-sapphire CMOS. *IEEE Trans. Circuits Syst. I* **53**, 2364–2370 (2006).
6. Weerakoon, P. et al. Patch-clamp amplifiers on a chip. *J. Neurosci. Methods* **192**, 187–192 (2010).
7. Kim, J., Maitra, R., Pedrotti, K. D. & Dunbar, W. B. A patch-clamp ASIC for nanopore-based DNA. *Anal. IEEE Trans. Biomed. Circuits Syst.* **7**, 285–295 (2013).
8. Li, H. et al. Ultracompact microwatt CMOS current readout with picoampere noise and kilohertz bandwidth for biosensor arrays. *IEEE Trans. Biomed. Circuits Syst.* **12**, 35–46 (2018).
9. Dai, S. & Rosenstein, J. K. A 15 V bidirectional current clamp circuit for integrated patch clamp electrophysiology. *IEEE Trans. Circuits Syst. II* **64**, 1287–1291 (2017).
10. Goldstein, B., Choe, K., Sigworth, F. J. & Culurciello, E. A four-channel integrated patch-clamp amplifier with current-clamp capability. In *Proceedings of Midwest Symposium on Circuits and Systems* 1–4 (IEEE, 2011).
11. Harrison, R. R. et al. Microchip amplifier for in vitro, in vivo and automated whole-cell patch-clamp recording. *J. Neurophysiol.* **113**, 1275–1282 (2014).
12. Sigworth, F. J. Design of the EPC-9, a computer-controlled patch-clamp amplifier. 1. Hardware. *J. Neurosci. Methods* **56**, 195–202 (1995).
13. Cole, K. S. *Membranes, Ions and Impulses: A Chapter of Classical Biophysics* (Univ. of California Press, 1972).
14. Larkum, M. E., Nevian, T., Sandier, M., Polsky, A. & Schiller, J. Synaptic integration in tuft dendrites of layer 5 pyramidal neurons: a new unifying principle. *Science* **325**, 756–760 (2009).
15. Jayant, K. et al. Targeted intracellular voltage recordings from dendritic spines using quantum-dot-coated nanopipettes. *Nat. Nanotechnol.* **12**, 335–342 (2017).
16. English, D. F. et al. Excitation and inhibition compete to control spiking during hippocampal ripples: intracellular study in behaving mice. *J. Neurosci.* **34**, 16509–16517 (2014).
17. Beaulieu-Laroche, L. & Harnett, M. T. Dendritic spines prevent synaptic voltage clamp. *Neuron* **97**, 75–82 (2018).
18. Razavi, B. *Design of Analog CMOS Integrated Circuits* (McGraw Hill, 2016).
19. Ferrari, G., Gozzini, F., Molari, A. & Sampietro, M. Transimpedance amplifier for high sensitivity current measurements on nanodevices. *IEEE J. Solid State Circuits* **44**, 1609–1616 (2009).
20. Ferrari, G., Farina, M., Guagliardo, F., Carminati, M. & Sampietro, M. Ultra-low-noise CMOS current preamplifier from DC to 1 MHz. *Electron. Lett.* **45**, 1278–1280 (2009).
21. Sherman, A. J., Shrier, A. & Cooper, E. Series resistance compensation for whole-cell patch-clamp studies using a membrane state estimator. *Biophys. J.* **77**, 2590–2601 (1999).
22. Long, M. A., Jin, D. Z. & Fee, M. S. Support for a synaptic chain model of neuronal sequence generation. *Nature* **468**, 394–399 (2010).
23. Perkins, K. L. Cell-attached voltage-clamp and current-clamp recording and stimulation techniques in brain slices. *J. Neurosci. Methods* **154**, 1–18 (2006).
24. Fromherz, P. Extracellular recording with transistors and the distribution of ionic conductances in a cell membrane. *Eur. Biophys. J.* **28**, 254–258 (1999).
25. Beaudoin, G. M. J. III et al. Culturing pyramidal neurons from the early postnatal mouse hippocampus and cortex. *Nat. Protoc.* **7**, 1741–1754 (2012).
26. Dingle, Y.-T. L. et al. Three-dimensional neural spheroid culture: an in vitro model for cortical studies. *Tissue Eng. Part C Methods* **21**, 1274–1283 (2015).

Acknowledgements

This work was supported in part by the National Institutes of Health under U01NS090596 and U01NS099697 to K.L.S.; UG3TR002151 to M.A.R. and R.T.; and R01MH101218, R01MH100561, DP1EY024503, R01EY011787 and R01NS110422 to R.Y. This work was also supported, in part, by the US Army Research Office under contract no. W911NF-12-1-0594 (MURI) and by DARPA under contract no. N66001-17-C-4002 to K.L.S. and R.Y. K.J. was supported in part by the Kavli Institute of Brain Science at Columbia.

Author contributions

S.S. and K.J. conceptualized the study and performed the experiments and analysis. S.S. designed the circuits. M.A.R. and R.T. provided cell cultures. R.Y. and K.L.S. provided advice on the experiments. K.L.S. provided overall supervision and guidance. S.S., K.J. and K.L.S. edited the manuscript. All authors provided comments.

Competing interests

S.S., K.J. and K.L.S. are listed as inventors on a provisional patent filed by Columbia University. The other authors declare no competing interests.

Additional information

Supplementary information is available for this paper at https://doi.org/10.1038/s41928-019-0285-3.

Reprints and permissions information is available at www.nature.com/reprints.

Correspondence and requests for materials should be addressed to K.J. or K.L.S.